

The Simons Observatory: forecasted constraints on primordial gravitational waves with the expanded array of Small Aperture Telescopes



The Simons Observatory Collaboration

I. Abril-Cabezas^{1,2} S. Adachi^{3,4} P. Ade,⁵ A. E. Adler^{6,7,8}
 P. Agrawal⁹ J. Aguirre¹⁰ S. Aiola¹¹ T. Alford^{12,13} A. Ali,⁶
 D. Alonso¹⁴ M. A. Alvarez,¹⁵ R. An,¹⁶ M. Aravena¹⁷
 K. Arnold^{18,9} P. Ashton,^{6,19,4} F. Astori,²⁰ Z. Atkins^{10,21}
 J. Austermann²² S. Azzoni²¹ C. Baccigalupi^{23,24,25}
 D. Baker,¹⁰ R. Balafendiev,²⁶ A. Baleato Lizancos^{6,15}
 D. Barron,²⁷ P. Barry,⁵ J. Bartlett,²⁸ A. Basyrov²⁸ N. Battaglia,²⁹
 E. S. Battistelli³⁰ R. Battye,³¹ A. Bayer,³² A. Bazarko²¹
 J. A. Beall²² R. Bean,²⁹ D. Beck,³³ S. Beckman,⁶ J. Begin,²¹
 A. Beheshti,³⁴ B. Beringue²⁸ T. Bhandarkar¹⁰ S. Bhimani¹²
 F. Bianchini,³⁵ E. Biermann,³⁴ M. Billi,³⁶ S. Biquard^{31,28}
 B. Bixler,⁹ L. Bizzarri,²⁰ S. Boada,³⁷ D. Boettger,⁹ B. Bolliet,^{38,2}
 J. R. Bond,³⁹ J. Borrill,^{19,40,10} J. Borrow,¹⁰ C. Braithwaite,⁵
 T. L. R. Brien⁵ M. L. Brown³¹ S. M. Bruno,²¹ S. Bryan⁴¹
 R. Bustos⁴² H. Cai,³⁴ E. Calabrese⁵ V. Calafut,²⁹ F. M. Carl,²¹
 A. Carones,²³ J. Carron,^{43,44} A. Challinor^{45,1,2} E. Chamberlain,⁴⁴
 P. Chanial,²⁸ N. Chen,⁴⁶ K. Cheung,³¹ B. Chiang^{47,48,49}
 Y. Chinone^{50,4} J. Chluba³¹ H. S. Cho,^{51,52} S. K. Choi⁵³
 M. Chu,⁹ J. Clancy³⁵ S. E. Clark^{33,51} P. Clarke,^{1,2} J. Cleary,¹²
 D. L. Clements⁵⁴ J. Connors,²² C. Contaldi^{55,54} G. Coppi,²⁰
 L. Corbett,⁶ N. F. Cothard,⁵⁶ W. Coulton^{2,1} D. Crichton,⁵⁷
 K. D. Crowley,²¹ K. T. Crowley,^{9,6} A. Cukierman,^{51,33,6}
 J. M. D'Ewart,⁵² N. Dachlythra²⁰ O. Darwish,⁴³ R. Datta¹²

S. Day-Weiss²¹ T. de Haan,⁵⁸ S. Desai,⁵ M. Devlin,¹⁰
L. Di Mascolo⁵⁹ S. Dicker¹⁰ K. Ding,⁶⁰ C. Doux,¹⁰ P. Dow,⁶¹
S. Doyle,⁵ C. J. Duell,⁶² S. M. Duff²² A. J. Duivenvoorden⁶³
J. Dunkley,^{21,32} M. Duparc,⁶⁴ D. Dutcher²¹ R. Dünner,⁶⁵
M. Edenton,⁶¹ H. El Bouhargani^{21,19} C. Embil Villagra,¹
J. Errard²⁸ G. Fabbian⁶⁶ V. Fanfani,²⁰ F. Farhadi Khouzani,⁶⁷
G. S. Farren^{19,68} J. Fergusson,^{1,2} S. Ferraro^{19,6} R. Flauger,⁹
M. Forconi^{69,70} A. Foster²¹ K. Freese^{71,72,73} J. C. Frisch,⁵¹
A. Frolov⁷⁴ G. Fuller,⁹ N. Galitzki^{71,72} P. A. Gallardo^{10,75}
G. Galloni^{70,69} J. T. Galvez Ghersi⁷⁶ K. Ganga²⁸
X. Garrido⁶⁴ E. Gawiser³⁷ M. Gerbino^{69,70} R. Gerras¹⁶
S. Giardiello⁵ A. Gill⁷⁷ V. Gilles,³¹ U. Giri,⁷⁸ E. Gleave,⁵⁴
V. Gluscevic¹⁶ N. Goeckner-Wald,⁶ S. Goldstein,⁷⁹
J. E. Golec⁸⁰ S. Gordon,⁴¹ M. Gralla⁸¹ S. Gratton,⁴⁵ D. Green,⁹
J. C. Groh¹⁵ C. Groppi,⁴¹ S. Grubb,¹⁰ Y. Guan^{82,83} N. Gupta,³⁵
J. E. Gudmundsson^{26,73} B. Hadzhiyska,⁶ S. Hagstotz,⁷³
P. Hargrave,⁵ S. Haridas,¹⁰ K. Harrington^{84,12} I. Harrison^{5,31}
M. Hasegawa^{58,50} M. Hasselfield,¹¹ V. Haynes,³¹
M. Hazumi^{58,85} A. He,¹⁶ E. Healy⁷⁵ S. W. Henderson^{51,52}
B. S. Hensley⁸⁶ E. Hertig^{45,2} C. Hervías-Caimapo⁶⁵
M. Higuchi,⁸⁷ C. A. Hill,^{6,19} J. C. Hill⁷⁹ M. Hilton^{88,57}
A. D. Hincks^{83,89} G. Hinshaw,⁹⁰ R. Hložek^{83,82} A. Y. Q. Ho⁶²
S. Ho,¹¹ S. P. Ho,³³ T. D. Hoang,⁹¹ J. Hoh,⁴¹ J. Holder,³¹
J. Hood,¹² E. Hornecker,⁸³ A. L. Hornsby,³¹ S. C. Hotinli⁷⁸
Z. Huang⁹² Z. B. Huber⁶² J. Hubmayr²²
K. Huffenberger^{47,48,49} A. Hughes^{47,48} J. P. Hughes,³⁷
A. Idicherian Lonappan⁹ M. Ikape,^{83,82} K. Inaba,⁸⁷ K. Irwin,^{51,33,52}
J. Iuliano,¹⁰ A. H. Jaffe,⁵⁴ B. Jain,¹⁰ D. Jain³¹ H. T. Jense⁵
O. Jeong,⁶ A. Johnson,⁹ B. R. Johnson⁶¹ M. Johnson,⁷⁸
M. E. Jones¹⁴ N. Joshi,¹⁰ B. Jost^{4,93} W. Kabalan²⁸
V. Kabra¹³ D. Kaneko⁵⁸ J. Kania,³¹ E. D. Karpel,³³
Y. Kasai⁹⁴ N. Katayama,⁴ B. Keating⁹ B. Keller⁶²
R. Keskitalo^{7,40,9} A. A. Khatua²⁶ J. Kim¹⁰ T. Kisner^{7,40}
K. Kiuchi,⁸⁷ K. Knowles,⁵⁷ A. M. Kofman^{10,12,75} Y. Koizumi,⁸⁷
B. J. Koopman⁹⁵ A. Kosowsky,³⁴ R. Kou⁴⁴
N. Krachmalnicoff,²³ D. Kramer,⁸¹ A. Krishak¹⁶ A. Krolewski,⁶
A. Kusaka^{87,19,4} A. Kusiak^{45,2} Y. Kvasiuk⁹⁶ P. La Plante⁶⁷
A. La Posta¹⁴ A. Laguë,¹⁰ A. Lai,⁹⁶ J. Lashner^{95,16}
M. Lattanzi^{69,70} A. Lee,^{6,19} E. Lee,^{10,31} J. Leech,¹⁴

L. Legrand^{1,2,97} **C. Lessler**^{13,75} **J. S. Leung**^{55,54} **A. Lewis**⁴⁴
Y. Li⁶² **Z. Li**^{68,15,39} **M. Limon**¹⁰ **L. Lin**⁶² **E. Linder**^{6,19}
M. Link²² **J. Liu**^{4,93} **Y. Liu**²¹ **J. Lloyd**⁷¹ **J. Lonergan**¹⁶
T. Louis⁶⁴ **T. Lucas**²² **M. Ludlam**⁴⁰ **M. Lungu**⁹⁸ **M. Lyons**⁵
N. MacCrann⁴⁵ **A. MacInnis**⁹⁹ **M. Madhavacheril**¹⁰ **D. Mak**⁵⁴
F. Maldonado⁴⁹ **M. Mallaby-Kay**¹² **A. Manduca**¹⁰ **A. Mangu**¹³
H. Mani⁴¹ **A. S. Maniyar**^{51,52} **G. A. Marques**¹⁰⁰ **P. Masson**²⁸
J. Mates²² **J. Mathewson**⁴¹ **T. Matsumura**^{4,93,87} **P. Mauskopf**⁴¹
A. May³¹ **N. McCallum**³¹ **H. McCarrick**²¹ **F. McCarthy**^{1,2,11}
M. McCrackan⁹⁵ **M. McCulloch**³¹ **J. McMahon**^{12,75,13,101,100}
P. D. Meerburg⁶⁰ **Y. Mehta**⁴¹ **J. Melin**^{28,102} **E. Meulbroek**¹²
J. Meyers¹⁰³ **A. Middleton**⁶² **Y. Miki**⁸⁷ **A. Miller**¹⁶
M. Mirmelstein⁴⁴ **Y. Mizozoe**⁹⁴ **B. Mohammadian**³¹
G. Montefalcone⁷¹ **K. Moodley**⁵⁷ **J. Moore**¹⁰⁴ **T. Morris**⁹⁵
M. Morshed^{69,70} **T. Morton**¹⁶ **E. Moser**⁶² **T. Mroczkowski**¹⁰⁵
M. Murata⁸⁷ **J. Myers**¹⁰ **M. Münchmeyer**⁹⁶ **S. Naess**¹⁰⁶
H. Nakata⁹⁴ **T. Namikawa**^{1,4,93,2} **M. Nashimoto**⁸⁷ **F. Nati**²⁰
P. Natoli^{70,69} **M. Negrello**⁵ **S. K. Nerval**^{83,82} **L. Newburgh**⁹⁵
D. V. Nguyen⁹⁵ **A. Nicola**³¹ **M. D. Niemack**^{62,29} **H. Nishino**⁸⁷
Y. Nishinomiya⁸⁷ **A. Novelli**²⁰ **S. O'Neill**²¹ **N. Okumoto**⁹⁴
A. Orlando³¹ **J. Orlowski-Scherer**¹⁰ **L. Pagano**^{70,69,66}
L. A. Page²¹ **S. Pandey**^{79,10} **A. Papageorgiou**⁵ **I. Paraskevacos**²¹
B. Partridge¹⁰⁷ **D. Patel**⁶² **R. Patki**²⁹ **S. Paulino Korte**⁴⁷
M. Peel⁵⁴ **K. Perez Sarmiento**¹⁰ **F. Perrotta**²³ **P. Phakathi**⁵⁷
L. Piccirillo³¹ **E. Pierpaoli**¹⁶ **T. Pinsonneault-Marotte**^{51,52}
G. Pisano³⁰ **J. Pitocco**¹² **D. Poletti**²³ **C. Popik**⁶² **B. Prasad**⁶
R. Puddu⁶⁵ **G. Puglisi**^{36,108,109} **F. J. Qu**^{51,52} **F. Rahman**^{47,48}
M. J. Randall⁶ **C. Ranucci**^{23,24,25} **C. Raum**⁶ **R. Reeves**¹¹⁰
C. L. Reichardt³⁵ **M. Remazeilles**¹¹¹ **X. Ren**²⁶ **Y. Rephaeli**¹¹²
D. Riechers²⁹ **B. Ried Guachalla**^{51,52} **A. Rizzieri**¹⁴ **J. Robe**¹⁰
M. F. Robertson⁴⁴ **N. Robertson**⁴⁵ **K. Rogers**⁸³ **F. Rojas**⁶⁵
A. Romero⁵² **E. Rosenberg**³¹ **A. Rotti**³¹ **S. Rowe**⁵ **A. Roy**²³
S. Sadeh¹¹² **N. Sailer**^{51,1} **K. Sakaguri**⁸⁷ **T. Sakuma**²¹
Y. Sakurai^{113,4} **M. Salatino**³³ **G. H. Sanders**^{98,114} **D. Sasaki**⁸⁷
M. Sathyanarayana Rao¹¹⁵ **T. P. Satterthwaite**¹⁰ **33,51**
L. J. Saunders^{12,100} **L. Scalcinati**²⁰ **E. Schaan**^{52,51} **B. Schmitt**¹⁰
M. Schmittfull¹¹⁶ **N. Sehgal**⁹⁹ **J. Seibert**⁹ **Y. Seino**^{21,94}
U. Seljak^{6,19} **S. Shaikh**⁴¹ **E. Shaw**^{71,72} **P. Shellard**^{1,2} **B. Sherwin**^{1,2}
M. Shimon¹¹² **J. E. Shroyer**^{61,117} **C. Sierra**^{51,52} **J. Sievers**⁵⁷

C. Sifón¹¹⁸ **P. Sikhosana**,⁵⁷ **M. Silva-Feaver**⁹⁵ **S. M. Simon**,¹⁰⁰
A. Sinclair,⁴¹ **K. Smith**,⁷⁸ **W. Sohn**,²⁸ **X. Song**,⁶ **R. F. Sonka**²¹,
T. Souverin,²⁰ **J. Spisak**,⁹ **S. T. Staggs**,²¹ **G. Stein**,^{6,19}
J. R. Stevens,⁶² **R. Stompor**,²⁸ **E. Storer**,²¹ **R. Sudiwala**,⁵
Y. Sueno²¹ **J. Sugiyama**⁸⁷ **P. Suman**,¹ **K. M. Surrao**⁷⁹,
S. Sutariya,¹³ **A. Suzuki**,¹⁹ **J. Suzuki**⁹⁴ **O. Tajima**^{94,58,4},
R. Takaku,⁵⁸ **S. Takakura**,^{94,4} **A. Takeuchi**,⁸⁷ **I. Tansieri**,⁷³
A. C. Taylor¹⁴ **G. Teply**,⁹ **T. Terasaki**,⁸⁷ **A. Thomas**^{12,75},
D. B. Thomas³¹ **R. Thornton**,¹⁰ **P. Timbie**,⁹⁶ **H. Trac**⁴⁶,
T. Tsan¹⁹ **E. Tsang King Sang**²⁸ **C. Tucker**⁵ **J. Ullom**²²,
L. Vacher²³ **L. Vale**,²² **A. van Engelen**,⁴¹ **J. Van Lanen**,²²
J. van Marrewijk¹¹⁹ **D. D. Van Winkle**,⁵² **C. Vargas**^{47,48},
E. M. Vavagiakis¹⁰⁴ **I. Veenendaal**,⁵ **C. Vergès**,²⁸
A. Villarrubia Aguilar²⁸ **M. Vissers**,²² **M. Viña**,⁵
K. Wagoner^{120,21} **S. Walker**,²² **L. Walters**,⁶¹ **Y. Wang**^{62,21},
B. Westbrook,⁶ **J. Williams**,³¹ **P. Williams**,¹⁹ **J. Wilson**,⁶¹
H. Winch,⁸³ **E. J. Wollack**¹²¹ **K. Wolz**¹⁴ **J. Wong**,³¹ **Z. Xu**¹²²,
K. Yamada^{21,87} **E. Young**,^{51,33} **B. Yu**,⁶ **C. Yu**,^{84,75} **G. Zagatti**^{70,69},
M. Zannoni,²⁰ **W. Zhang**,¹⁴ **K. Zheng**²¹ **N. Zhu**,¹⁰ **A. Zonca**¹²³,
and **I. Zubeldia**^{1,2}

¹DAMTP, Centre for Mathematical Sciences, University of Cambridge, Wilberforce Road, Cambridge CB3 OWA, UK

²Kavli Institute for Cosmology Cambridge, Madingley Road, Cambridge CB3 0HA, UK

³Okayama University, Department of Physics, Okayama 700-8530, Japan

⁴Kavli IPMU (WPI), UTIAS, The University of Tokyo, Kashiwa, Chiba 277-8583, Japan

⁵School of Physics and Astronomy, Cardiff University, UK

⁶Department of Physics, University of California Berkeley, Berkeley, CA, USA

⁷Computational Cosmology Center, Lawrence Berkeley National Laboratory, Berkeley, CA, USA

⁸CNRS-UCB International Research Laboratory, Centre Pierre Binétruy, IRL2007, CPB-IN2P3, Berkeley, US

⁹Department of Physics, University of California San Diego, San Diego, CA, USA

¹⁰Department of Physics and Astronomy, University of Pennsylvania, Philadelphia, PA 19104 USA

¹¹Center for Computational Astrophysics, Flatiron Institute, USA

¹²Department of Astronomy and Astrophysics, University of Chicago, 5640 South Ellis Avenue, Chicago, IL, 60637, USA

¹³University of Chicago, Department of Physics, 5720 S Ellis Ave, Chicago, IL, 60637, USA

¹⁴Department of Physics, University of Oxford, Denys Wilkinson Building, Keble Road, Oxford OX1 3RH, United Kingdom

¹⁵Lawrence Berkeley National Laboratory, Berkeley, CA, USA

¹⁶Department of Physics and Astronomy, University of Southern California, Los Angeles, CA 90089-1483 USA

¹⁷Instituto de Estudios Astrofísicos, Universidad Diego Portales, Av. Ejercito Libertador 441, Santiago, Chile

¹⁸Department of Astronomy & Astrophysics, University of California San Diego, San Diego, CA, USA

¹⁹Physics Division, Lawrence Berkeley National Laboratory, Berkeley, CA, USA

²⁰Department of Physics, University of Milano-Bicocca, Piazza della Scienza 3, 20126 Milano (MI), Italy

²¹Department of Physics, Princeton University, Jadwin Hall, Princeton, NJ 08544, USA

²²Quantum Sensors Division, National Institute of Standards and Technology, 325 Broadway, Boulder, CO 80305

²³The International School for Advanced Studies (SISSA), via Bonomea 265, I-34136 Trieste, Italy

²⁴The National Institute for Nuclear Physics (INFN), via Valerio 2, I-34127, Trieste, Italy

²⁵Institute for Fundamental Physics of the Universe (IFPU), Via Beirut 2, 34151, Trieste, Italy

²⁶Science Institute, University of Iceland, 107 Reykjavik, Iceland

²⁷Department of Physics and Astronomy, University of New Mexico, USA

²⁸Université Paris Cité, CNRS, Astroparticule et Cosmologie, F-75013 Paris, France

²⁹Department of Astronomy, Cornell University, Ithaca, NY 14853, USA

³⁰Department of Physics, Sapienza University of Rome

³¹Jodrell Bank Centre for Astrophysics, Department of Physics and Astronomy, University of Manchester, Manchester M13 9PL, UK

³²Department of Astrophysical Sciences, Payton Hall, Princeton University, Princeton, NJ 08544, USA

³³Department of Physics, Stanford University, USA

³⁴Department of Physics and Astronomy, University of Pittsburgh

³⁵School of Physics, The University of Melbourne, Parkville VIC 3010, Australia

³⁶Dipartimento di Fisica e Astronomia, Università degli Studi di Catania, via S. Sofia, 64, 95123, Catania, Italy

³⁷Department of Physics and Astronomy, Rutgers, the State University of New Jersey, Piscataway, NJ, USA

³⁸Astrophysics Group, Cavendish Laboratory, J. J. Thomson Avenue, Cambridge CB3 0HE, United Kingdom

³⁹Canadian Institute for Theoretical Astrophysics, University of Toronto, 60 St. George St., Toronto, ON M5S 3H8, Canada

⁴⁰Space Sciences Laboratory, University of California Berkeley, Berkeley, CA, USA

⁴¹School of Earth and Space Exploration, Arizona State University, Tempe, AZ, 85287

⁴²Departamento de Ingeniería Eléctrica, Universidad Católica de la Santísima Concepción, Alonso de Ribera 2850, Concepción, Chile

⁴³Université de Genève, Département de Physique Théorique et CAP, 24 Quai Ansermet, CH-1211 Genève 4, Switzerland

⁴⁴Department of Physics & Astronomy, University of Sussex, Brighton BN1 9QH, UK

⁴⁵Institute of Astronomy, University of Cambridge, Madingley Road, Cambridge CB3 0HA, UK

⁴⁶McWilliams Center for Cosmology and Astrophysics, Department of Physics, Carnegie Mellon University, USA

⁴⁷Department of Physics & Astronomy, Texas A&M University, College Station, TX 77843, USA

⁴⁸Mitchell Institute for Fundamental Physics & Astronomy, Texas A&M University, College Station, TX 77843, USA

⁴⁹Department of Physics, Florida State University, Tallahassee, FL 32306 USA

⁵⁰QUP (WPI), KEK, Tsukuba, Ibaraki 305-0801, Japan

⁵¹Kavli Institute for Particle Astrophysics & Cosmology, 452 Lomita Mall, Stanford, CA 94305, USA

⁵²SLAC National Accelerator Laboratory, 2575 Sand Hill Road, Menlo Park, California 94025, USA

⁵³Department of Physics and Astronomy, University of California, Riverside, CA 92521, USA

⁵⁴Blackett Laboratory, Imperial College London, Prince Consort Road, London SW7 2AZ, UK

⁵⁵Abdus Salam Centre for Theoretical Physics, Imperial College London, London SW7 2AZ, UK

⁵⁶Department of Applied and Engineering Physics, Cornell University, Ithaca, NY 14853, USA

⁵⁷Astrophysics Research Centre, School of Mathematics, Statistics, and Computer Science, University of KwaZulu-Natal, Westville Campus, Durban 4041, South Africa

⁵⁸High Energy Accelerator Research Organization (KEK), Tsukuba, 305-0801, Japan

⁵⁹Kapteyn Astronomical Institute, University of Groningen, Landleven 12, 9747 AD, Groningen, The Netherlands

⁶⁰Van Swinderen Institute for particle physics and gravity, Nijenborgh 3, 9747 AG Groningen, The Netherlands

⁶¹Department of Astronomy, University of Virginia, Charlottesville, VA 22904, USA

⁶²Department of Physics, Cornell University, Ithaca, NY 14853, USA

⁶³Max-Planck-Institut für Astrophysik, Karl-Schwarzschild Str. 1, 85741 Garching, Germany

⁶⁴Université Paris-Saclay, CNRS/IN2P3, IJCLab, 91405 Orsay, France

⁶⁵Instituto de Astrofísica and Centro de Astro-Ingeniería, Facultad de Física, Pontificia Universidad Católica de Chile, Chile

⁶⁶Institut d’Astrophysique Spatiale, CNRS, Univ. Paris-Sud, Université Paris-Saclay, Bât. 121, 91405 Orsay cedex, France

⁶⁷Nevada Center for Astrophysics, University of Nevada Las Vegas, Las Vegas, NV 89154, USA

⁶⁸Berkeley Center for Cosmological Physics, University of California, Berkeley, CA 94720, USA

⁶⁹Istituto Nazionale di Fisica Nucleare, Sezione di Ferrara, via Saragat 1, I-44122 Ferrara, Italy

⁷⁰Dipartimento di Fisica e Scienze della Terra, Università degli Studi di Ferrara, via Saragat 1, I-44122 Ferrara, Italy

⁷¹Department of Physics, University of Texas at Austin, Austin, TX, 78712, USA

⁷²Weinberg Institute for Theoretical Physics, Texas Center for Cosmology and Astroparticle Physics, Austin, TX 78712, USA

⁷³The Oskar Klein Centre for Cosmoparticle Physics, Department of Physics, Stockholm University, AlbaNova, SE-106 91 Stockholm, Sweden

⁷⁴Physics Department, Simon Fraser University

⁷⁵Kavli Institute for Cosmological Physics, University of Chicago, 5640 S Ellis Ave, Chicago, IL, 60637, USA

⁷⁶Universidad de Ingenieria y Tecnologia, Jr. Medrano Silva 165, Barranco, Lima, Perú

⁷⁷Department of Aeronautics and Astronautics, Massachusetts Institute of Technology, 77 Massachusetts Avenue, Cambridge, MA 02139, USA

⁷⁸Perimeter Institute for Theoretical Physics, 31 Caroline Street N, Waterloo ON N2L 2Y5, Canada

⁷⁹Department of Physics, Columbia University, New York, NY 10027, USA

⁸⁰Department of Astronomy, University of Massachusetts Amherst, 710 N Pleasant St, Amherst, MA 01003

⁸¹Department of Astronomy/Steward Observatory, University of Arizona, 933 N. Cherry Ave., Tucson, AZ 85721, USA

⁸²Dunlap Institute for Astronomy & Astrophysics, University of Toronto, 50 St. George St., Toronto ON M5S 3H4, Canada

⁸³David A. Dunlap Department of Astronomy and Astrophysics, University of Toronto, 50 St. George St., Toronto ON M5S 3H4, Canada

⁸⁴Argonne National Laboratory, High Energy Physics Division. 9700 S Cass Ave, Lemont, IL, 60439, USA

⁸⁵Department of Physics and Center for High Energy and High Field Physics (CHeP), National Central University, Taoyuan City, Taiwan

⁸⁶Jet Propulsion Laboratory, California Institute of Technology, 4800 Oak Grove Drive, Pasadena, CA 91109, USA

⁸⁷Department of Physics, The University of Tokyo, Tokyo 113-0033, Japan

⁸⁸Wits Centre for Astrophysics, School of Physics, University of the Witwatersrand, Private Bag 3, 2050, Johannesburg, South Africa

⁸⁹Specola Vaticana (Vatican Observatory), V-00120 Vatican City State

⁹⁰Department of Physics and Astronomy, University of British Columbia, Vancouver, BC, Canada

⁹¹School of Physics and Astronomy, University of Minnesota, Minneapolis, MN 55455, USA

⁹²School of Physics and Astronomy, Sun Yat-sen University, 2 Daxue Road, Zhuhai, 519082, China

⁹³Center for Data-Driven Discovery, Kavli IPMU (WPI), UTIAS, The University of Tokyo, Kashiwa, Chiba 277-8583, Japan

⁹⁴Department of Physics, Faculty of Science, Kyoto University, Kyoto 606-8502, Japan

⁹⁵Wright Laboratory, Department of Physics, Yale University, New Haven, Connecticut 06511, USA

⁹⁶Department of Physics, University of Wisconsin-Madison, Madison, WI 53706, USA

⁹⁷Centro Brasileiro de Pesquisas Físicas (CBPF), Rua Doutor Xavier Sigaud 150, 22290-180, Rio de Janeiro, Brazil

⁹⁸Simons Observatory

⁹⁹Physics and Astronomy Department, Stony Brook University, Stony Brook, NY 11794, USA

¹⁰⁰Fermi National Accelerator Laboratory, Batavia, IL 60510, USA

¹⁰¹University of Chicago, Enrico Fermi Institute, 5640 S Ellis Ave, Chicago, IL, 60637, USA

¹⁰²Université Paris-Saclay, CEA, Département de Physique des Particules, 91191, Gif-sur-Yvette, France

¹⁰³Department of Physics, Southern Methodist University, USA

¹⁰⁴Department of Physics, Duke University, Durham, NC 27710, USA

¹⁰⁵Institute of Space Sciences (ICE, CSIC), Carrer de Can Magrans, s/n, 08193 Cerdanyola del Vallès, Barcelona, Spain

¹⁰⁶Institute for theoretical astrophysics, University of Oslo, Norway

¹⁰⁷Department of Physics and Astronomy, Haverford College, 370 Lancaster Ave, Haverford, PA 19041, USA

¹⁰⁸The National Institute for Nuclear Physics INFN - Via S. Sofia 64, 95123 Catania, Italy

¹⁰⁹INAF - Osservatorio Astrofisico di Catania, via S. Sofia 78, 95123 Catania, Italy

¹¹⁰Departamento de Astronomía, Universidad de Concepción, Victor Lamas 1290, Concepción, Chile

¹¹¹Instituto de Fisica de Cantabria (CSIC-UC), Avenida de los Castros s/n, 39005 Santander, Spain

¹¹²School of Physics and Astronomy, Tel Aviv University, Tel Aviv, 69978, Israel

¹¹³Faculty of Engineering, Department of Mechanical and Electrical Engineering, 5000-1, Toyohira, Chino-shi, Nagano, 391-0292, Japan

¹¹⁴Project Science LLC, 572 Alta Vista Way, Laguna Beach, CA 92651 USA

¹¹⁵Raman Research Institute, Bengaluru, India

¹¹⁶PDT Partners, 60 Columbus Circle, New York, NY 10023, USA

¹¹⁷National Radio Astronomy Observatory, 520 Edgemont Road, Charlottesville, VA 22903, USA

¹¹⁸Instituto de Física, Pontificia Universidad Católica de Valparaíso, Casilla 4059, Valparaíso, Chile

¹¹⁹Leiden Observatory, Leiden University, P.O. Box 9513, 2300 RA Leiden, The Netherlands

¹²⁰Department of Physics, North Carolina State University

¹²¹NASA / Goddard Space Flight Center, Greenbelt, MD 20771, USA

¹²²MIT Kavli Institute, Massachusetts Institute of Technology, 77 Massachusetts Avenue, Cambridge, MA 02139, USA

¹²³San Diego Supercomputer Center, University of California San Diego, La Jolla, CA, USA

E-mail: so_publications@simonsobservatory.org

Abstract. We present updated forecasts for the scientific performance of the degree-scale (0.5 deg FWHM at 93 GHz), deep-field survey to be conducted by the Simons Observatory (SO). By 2027, the SO Small Aperture Telescope (SAT) complement will be doubled from three to six telescopes, including a doubling of the detector count in the 93 GHz and 145 GHz channels to 48,160 detectors. Combined with a planned extension of the survey duration to 2035, this expansion will significantly enhance SO's search for a *B*-mode signal in the polarisation of the cosmic microwave background, a potential signature of gravitational waves

produced in the very early Universe. Assuming a $1/f$ noise model with knee multipole $\ell_{\text{knee}} = 50$ and a moderately complex model for Galactic foregrounds, we forecast a 1σ (or 68% confidence level) constraint on the tensor-to-scalar ratio r of $\sigma_r = 1.2 \times 10^{-3}$, assuming no primordial B -modes are present. This forecast assumes that 70% of the B -mode lensing signal can ultimately be removed using high resolution observations from the SO Large Aperture Telescope (LAT) and overlapping large-scale structure surveys. For more optimistic assumptions regarding foregrounds and noise, and assuming the same level of delensing, this forecast constraint improves to $\sigma_r = 7 \times 10^{-4}$. These forecasts represent a major improvement in SO’s constraining power, being a factor of around 2.5 times better than what could be achieved with the originally planned campaign, which assumed the existing three SATs would conduct a five-year survey.

1 Introduction

The Simons Observatory (SO) is a new millimetre-wave (mm) observatory that has recently started scientific operations from its high-altitude site in the Atacama Desert of northern Chile. SO currently consists of one Large Aperture Telescope (LAT, a 6 m diameter reflecting telescope) and three Small Aperture Telescopes (SATs, each consisting of a 0.42 m refractive aperture). The scientific reach of SO is wide ranging, and a comprehensive overview is presented in [SO Collaboration \(2019\)](#). Detailed descriptions of the instrumentation already deployed on the SO site are presented in [Xu et al. \(2021\)](#), [Zhu et al. \(2021\)](#), [Galitzki et al. \(2024\)](#), and [Bhandarkar et al. \(2025\)](#).

The SO programme is being enhanced in several ways beyond the capabilities described in [SO Collaboration \(2019\)](#). This paper focuses on the 0.42 m SATs and the science enabled via the degree-scale, deep survey that they are undertaking. In this regard, the major improvement programme, which is underway and already well advanced, consists of doubling the number of SATs from three to six telescopes. The other SO enhancements are described in [SO Collaboration \(2025\)](#).

As described in [SO Collaboration \(2019\)](#), the SO SATs are designed to pursue a key science goal — the search for a B -mode polarisation signal on large angular scales in the cosmic microwave background (CMB) radiation. A detection of this signal would provide compelling evidence that primordial gravitational waves were generated in the very early universe ([Kamionkowski et al. 1997](#); [Seljak & Zaldarriaga 1997](#)). This search for “primordial B -modes” is amongst the most prominent goals of modern observational cosmology and, in addition to SO, is being pursued by multiple ground-based, balloon, and satellite experiments (e.g. [Addamo et al. 2021](#); [Ade et al. 2022](#); [Battistelli et al. 2020](#); [Ghosh et al. 2022](#); [Harrington et al. 2016](#); [Hui et al. 2018](#); [LiteBIRD Collaboration 2023](#); [Zebrowski et al. 2025](#)).

In this paper, we present an update to the constraints that SO is forecasted to achieve on the tensor-to-scalar ratio, r , taking into account the expansion of the SAT complement from three to six telescopes, and an extension of the survey duration to ten years. To produce these forecasts, we have adopted the same assumptions regarding key instrument parameters as were assumed in our previous forecasting work ([SO Collaboration 2019](#)). In particular, we have used the same per-detector white noise levels and the same full-width at half maximum (FWHM) model instrument beam widths as used in [SO Collaboration \(2019\)](#). These design values for the beam FWHMs and the predicted map-level noise for the expanded 10-year, six-SAT survey configuration are presented in Table 1. The realised values for these parameters, as measured from calibration observations with the already-deployed SATs, and

a comparison of the measured performance with the design parameters used here, will be presented in forthcoming publications.

The remainder of this paper is organised as follows. In Section 2, we briefly describe the expanded SAT infrastructure and the extended deep-field survey. In Section 3, we forecast the primary scientific analyses that will be enabled by this programme. Much of the forecasting methodology used here is similar or identical to that employed in the SO science goals and forecasts paper (SO Collaboration 2019) or the complementary SO Galactic science goals and forecasts paper (Hensley et al. 2022). We direct the interested reader to those papers for further details. In Section 4, we conclude and discuss the outlook for SO operations and science.

2 Expanded capabilities

The three SO SATs already deployed on the site include two “mid-frequency” (MF) SATs, operating at 93 and 145 GHz, and one “ultra-high-frequency” (UHF) SAT, operating at 225 and 280 GHz. The ongoing programme to add to this infrastructure consists of one effort to build and deploy two further MF SATs (part of the wider SO:UK project) and a second programme to build and deploy a single “low-frequency” (LF) SAT operating at 27 and 39 GHz.¹ The LF SAT is being delivered, in part, by the Japan-SAT (JSAT) project. The two additional MF SATs will each field 12,040 detectors (the same as the deployed MF SATs) and will thus double the mapping speed of the SO SAT facility at the central CMB frequencies of 93/145 GHz. The LF SAT will add observational capability at lower frequencies, which will be helpful for characterising and removing Galactic synchrotron emission, a prevalent foreground contaminant in CMB observations (Hensley et al. 2022; SO Collaboration 2019). Once completed, the three additional SATs will increase the total number of deployed detectors on SO SATs to 61,852.

The two additional MF receivers mostly follow the design of the original MF SATs, though there are some differences. The most significant difference is that the new MF SATs will use kinetic inductance detectors (KIDs) in place of the transition edge sensors (TESs) used in all of the other SO telescopes. KIDs (Day et al. 2003; Doyle et al. 2008) are much simpler to read out than TESs and are thus, potentially, a key enabling technology for future CMB and mm-wave facilities planning to field instruments with many thousands of detectors. The two new SO MF SATs are expected to be the first demonstration of horn-coupled, orthomode transducer (OMT) dichroic KIDs on a deployed instrument. The KID arrays will be complemented by simple digital readout systems, based on radio frequency system-on-chip (RFSoC) technology (see e.g. Liu et al. 2021). These readout units will be used in place of the SMuRF systems (Yu et al. 2023) used by the other SO telescopes. The second significant difference is the implementation of a simplified two-lens optical design in the new MF SATs instead of the three-lens system used in the other SO SATs (Galitzki et al. 2024). Note that the LF SAT is based on a three-lens optical design and will use TES detectors and SMuRF readout as per the first three SO SATs.

Table 1 details how the 61,852 SO SAT detectors are distributed across frequencies. The table also presents the forecasted map white noise levels for an extended-duration SO SAT

¹The originally envisaged SO SAT configuration included three telescope platforms (mounts) and four receivers – two MF, one UHF and one LF. The previous plan was to exchange one of the MF receivers with the LF receiver for one year of operations. Under the enhanced SAT programme the LF receiver will be deployed on its own dedicated telescope platform and no exchange of receivers will be necessary.

Table 1. SO Small Aperture Telescopes Survey Specifications

Frequency [GHz]	FWHM [arcmin]	Baseline Depth [$\mu\text{K} \cdot \text{arcmin}$]	Goal Depth [$\mu\text{K} \cdot \text{arcmin}$]	Frequency Bands	Detector Count	Int. time [SAT · years]
27	91	16	12	LF	826	8
39	63	10	7.7		826	
93	30	1.7	1.2	MF	24,080	36.5
145	17	2.1	1.4		24,080	
225	11	5.9	3.9	UHF	6,020	10
280	9	15	9.6		6,020	

Design instrument parameters used for the forecasts presented in this paper. The white noise levels (“depth”) are provided for polarisation, for the fully completed, ten-year SO SAT survey. Two sensitivity targets are presented (baseline and goal), as in [SO Collaboration \(2019\)](#). Note that [SO Collaboration \(2019\)](#) provided depth levels for total intensity, which are a factor $1/\sqrt{2}$ smaller than the corresponding polarisation noise levels. Besides this, and the different number of telescopes and observing time, the depth levels quoted here also account for the impact of inhomogeneous noise as described in [Wolz et al. \(2024\)](#). The right-most column presents the total integration time as “SAT-years” where one SAT-year corresponds to one SAT observing for one calendar year. The noise model assumes an observing efficiency of 20%, based on past achieved performance (see [SO Collaboration 2019](#)). Note also that the additional MF SATs will make use of KIDs instead of TESs (see main text for further details).

survey, covering approximately 10% of the sky and projected to finish in 2035. For simplicity, these forecasted noise levels assume identical performance for both KIDs and TESs.

All three additional SATs will use existing infrastructure from the Atacama Cosmology Telescope (ACT, [Swetz et al. 2011](#)) and POLARBEAR/Simons Array experiments ([Lee et al. 2008](#); [Stebor et al. 2016](#)) at the SO site. The LF SAT will be deployed on the site previously occupied by ACT, and will modify and re-use the ACT ground screen. The two additional MF SATs will be deployed on the site previously occupied by the POLARBEAR and Simons Array telescopes. These two MF SATs will be surrounded by new purpose-built ground screens. At the time of writing the construction of this additional site infrastructure is nearing completion.

All of the new components are planned to be complete by 2027 (see timeline in Fig. 1). Observations with the first two MF SATs are already underway and the UHF SAT is currently in commissioning. For the forecasts presented in this paper, we assume a cumulative survey duration of 10 years. For the first two years, we assume operation with the original three SO SATs, and for the subsequent eight years we assume operation with the full complement of six SATs. The forecasts presented in Sec. 3 are based on the cumulative sensitivity of the entire survey, accounting for the sensitivity improvement at the transition between three and six SATs. Our forecasting approach follows that explained in detail in [SO Collaboration \(2019\)](#). We refer the reader to that paper for further details.

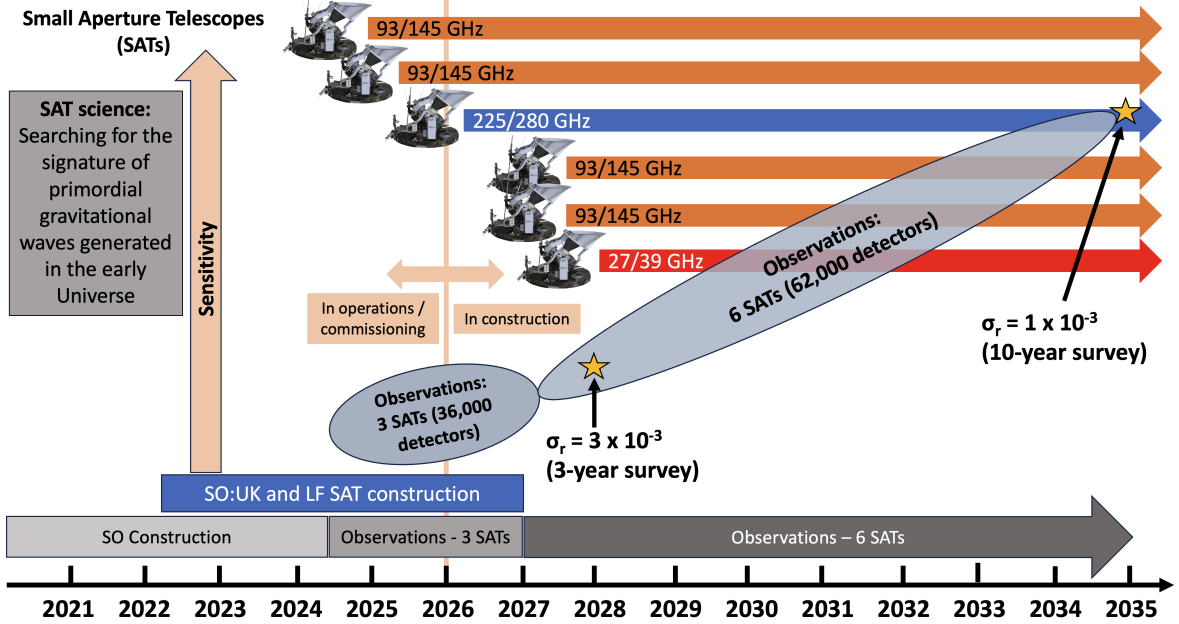


Figure 1. Timeline of the Simons Observatory expanded SATs programme. Two additional “mid-frequency” SATs, operating at 93/145 GHz, are due to begin operations in 2027. A sixth “low-frequency” SAT, operating at 27/39 GHz is due to commence operations on a similar timescale. The additional telescopes, combined with an extension of the SO SAT survey to the mid-2030s, will significantly enhance the scientific reach of the observatory. This is demonstrated here by quoting forecasts for the errors achieved on the tensor-to-scalar ratio, σ_r , by 2028 and by 2035. For clarity, forecasted errors are quoted only for the “pessimistic” $1/f$ noise model, assuming a moderately complex model for astrophysical foregrounds (i.e. allowing for foreground frequency decorrelation – see text in Section 3 for details). See Figure 3 and Table 2 for the detailed forecasting results, covering a wider range of assumptions for the levels of noise, foreground complexity and delensing achieved.

3 Forecasts

3.1 Forecasting framework

To quantify the sensitivity of the upgraded SAT complement to primordial gravitational waves, and to compare it with the constraints achievable by SO before this upgrade, we carry out forecasts following the approach described in [Wolz et al. \(2024\)](#) (W24 hereafter). More concretely, we adopt a multi-frequency power-spectrum-based component separation strategy (“Pipeline A” in the language of W24), in which the contributions from all polarised sky components (CMB and Galactic foregrounds) are forward-modelled to the set of all auto- and cross-spectra between the 6 frequency channels observed by SO. This aligns with the main strategy used for the analysis of current SO data, as well as the approach taken by previous experiments ([BICEP2/Keck Collaborations 2018](#)). We use only angular multipoles in the range $\ell \in [30, 300]$, and assume a Gaussian likelihood for the measured spectra, which was found by W24 to be a good approximation in this range of scales. Further details of the pipeline implementation can be found in W24 and references therein. A validation of this approach in the presence of realistic timestream filtering and inhomogeneous noise was recently presented in [Hervías-Caimapo et al. \(2025\)](#). Most of the assumptions adopted for these forecasts are the same as those used in W24, in order to facilitate a comparison with

previous forecasts for the nominal SO configuration.²

We assume the same survey strategy, resulting sky footprint and apodised mask used in W24, as well as the same noise model, characterising the contributions of white and correlated $1/f$ noise. The resulting footprint has a sky fraction of approximately $f_{\text{sky}} = 0.10$.³ The amplitude of the resulting noise power spectra at different frequencies are then scaled according to the sensitivity achieved by a given SAT configuration (e.g. the upgraded SAT complement after a given integration time). In particular, we assume the “baseline” white noise levels (see Table 1), and we produce forecasts for the two $1/f$ noise models labelled “pessimistic” and “optimistic” in [SO Collaboration \(2019\)](#), and in W24. For guidance, the “pessimistic” and “optimistic” noise models assume knee multipole scales $\ell_{\text{knee}} = 50$ and 25, respectively. We assume identical sensitivity for all four MF SATs. To produce forecasts for the error on the tensor-to-scalar ratio r as a function of the total integration time, we assume the following schedule for the deployment of the different SO SATs:

- At the start of the first year, the three nominal SO SATs (two of them targeting the MF bands, and one targeting the UHF bands) have been deployed.
- The first additional MF SAT starts observations half-way through the second year.
- The second additional MF SAT, and the additional LF SAT start observations at the start of the third year.

We further assume that all telescopes will continue observations until 2035 (i.e. a total of 10 years for the nominal SATs). With this setup, at the end of the fifth year of observations, the enhanced SO SATs will have accumulated a total of 3, 16.5, and 5 telescope-years of observations in the LF, MF, and UHF channels, respectively (compared to 1, 9, and 5 for nominal SO). After the 10-year survey, the accumulated sensitivity would be 8, 36.5, and 10 telescope-calendar years, in the same channels. The noise model used assumes a 20% observing efficiency. We emphasise that the forecasts presented in the next section depend critically on the assumed observing schedule and noise properties. They also do not account for unmodeled instrumental systematic effects. While these assumptions are based on reasonably realistic expectations, it is impossible to guarantee that they will match the final deployment schedule and instrumental performance of such a complex experiment.

As in W24, we generate a suite of simulations, each incorporating the contribution from CMB, foregrounds, and instrumental noise. The latter is both inhomogeneous and non-white (the procedure used to generate noise realisations is described in [SO Collaboration 2019](#), and in W24). The CMB contribution to the B -mode signal consists solely of lensed E -modes, assuming no primordial B -modes ($r = 0$). To replicate the effects of delensing, we simply scale the lensing B -mode power spectrum by an amplitude parameter, A_{lens} , which quantifies the level of lensing residuals remaining in the B -mode power spectrum, following the application of delensing procedures. Removing approximately 50% of the lensing B -mode

²As SO has progressed, some of these assumptions have been revised. In particular, the scanning strategy used to define the hits map used in W24 has been updated over several iterations. We have verified that, in the most stringent case (i.e. for the 10-year survey with $A_{\text{lens}} = 0.3$), the forecast uncertainties on r reported in the next section vary by less than 10% if analysed using the most up-to-date scanning strategy, the details of which are still under development.

³This is estimated as $f_{\text{sky}} = \langle N_{\text{hits}}^2 \rangle / \langle N_{\text{hits}}^4 \rangle$, where N_{hits} is the hits count map corresponding to the selected survey strategy, and $\langle \cdot \rangle$ denotes averaging over the sky. This definition of f_{sky} is appropriate in the signal-dominated regime. In the noise-dominated regime, a more appropriate estimate is $f_{\text{sky}}^N = \langle N_{\text{hits}} \rangle^2 / \langle N_{\text{hits}}^2 \rangle$, which is approximately $f_{\text{sky}} = 0.18$ for the scanning strategy assumed here.

power (i.e. $A_{\text{lens}} = 0.5$) should be feasible using external tracers of the large-scale structure as lensing templates (Planck Collaboration 2020b; Yu et al. 2017). This can be further improved through “internal” delensing (i.e. using the lensing potential reconstructed from high-resolution CMB observations), given enough sensitivity. Namikawa et al. (2022) and Hertig et al. (2024) showed that the nominal SO observations should be able to achieve 65% efficiency ($A_{\text{lens}} = 0.35$). An extended observational campaign with the SO LAT, such as that described in SO Collaboration (2025), would be able to improve this further. Thus, we produce forecasts for $A_{\text{lens}} = 0.5$ and $A_{\text{lens}} = 0.3$, bracketing the range of delensing efficiencies that SO could achieve, depending on the sensitivity of the LAT data. Note that we do not attempt to incorporate delensing as part of the analysis (e.g. incorporating it as part of the multi-frequency likelihood as done in Hertig et al. 2024), but instead mimic its impact by assuming that a fraction of the lensing B -mode power has been subtracted from the maps. This has been shown to be a reasonable approximation for forecasting (Hertig et al. 2024).

We use simple Gaussian realisations with spatially-constant spectral indices to simulate the contribution from Galactic foregrounds. These are the same Gaussian foreground simulations described in W24. This approach neglects a number of important foreground properties, including their intrinsic spatial inhomogeneity and non-Gaussianity, spatially-varying spectra, and other sources of frequency decorrelation (Hensley et al. 2022; Jung et al. 2018; Martínez-Solaeche et al. 2018; The Pan-Experiment Galactic Science Group 2025; von Hausegger et al. 2019; Wang et al. 2020). However, we incorporate the most important of these effects in the model used to fit the simulated data. This allows us to account for the impact of marginalising over the additional degrees of freedom needed to describe these effects on the final uncertainties on r , while ignoring the impact of varying foreground complexity on its central value, and avoiding the exploration of different foreground templates of varying complexity. As shown in W24, the impact of foregrounds on the forecast σ_r is dominated by the level of complexity assumed in the model used for component separation, and not in the particular foreground model used to generate the simulated data (assuming unbiased constraints and adequate model complexity). A more in-depth study of foreground complexity for nominal SO is presented in W24, where the model used here was shown to be sufficiently flexible to recover unbiased constraints on r in the presence of reasonably complex foreground models. See also the more recent work of Liu et al. (2025). We include the contribution from Galactic synchrotron emission, assuming a power-law spectrum with spectral index $\beta_s = -3$, and Galactic polarised dust, characterised by a modified black-body spectrum with temperature $T_d = 20$ K, and a spectral index, $\beta_d = 1.54$ (Thorne et al. 2017, W24). Maps for both components at their pivot frequencies (23 GHz for synchrotron and 353 GHz for dust, respectively) were generated assuming power-law power spectra, with amplitude and spectral tilt parameters calibrated to reproduce the level of contamination present in the assumed sky footprint (see W24 for details).

We generate 500 realisations of the signal components (CMB and foregrounds), convolved at each frequency with a Gaussian instrumental beam (see Table 1). We combine them with the noise realisations described above to generate simulated observations assuming different levels of instrumental sensitivity. These noise realisations are generated directly at the map level, using the same noise power spectrum model described in W24, as well as the procedure described there to account for noise inhomogeneity. These noise curves were designed to account for the impact of time-domain filtering, and we further discard all multipoles below $\ell = 30$ to avoid scales that are likely affected by atmospheric noise and aggressive filtering.

Specifically, we create simulations for the nominal SO sensitivity after 5 years of observations, as well as for the enhanced SO SAT complement every year through a 10-year observing campaign. We measure the angular power spectra of all sky realisations, and use the 500 independent simulations to construct a multi-frequency power spectrum covariance, to be used in the component separation likelihood. As in W24, we set all elements of this covariance matrix corresponding to pairs of distinct angular bandpowers to zero,⁴ in order to reduce the numerical noise in the covariance. Although this neglects the small statistical correlation within such bandpower pairs, W24 found this to be negligible. All power spectra were estimated with `NaMaster` (Alonso et al. 2019), making use of B -mode purification to eliminate the impact of E -to- B leakage in the power spectrum uncertainties (Smith 2006). We use bandpowers of width $\Delta\ell = 10$, and discard all multipoles outside the range $\ell \in [30, 300]$.

As described above, all sky components are modelled at the power spectrum level, using the model described in W24. This includes two CMB parameters, r and A_{lens} , characterising the amplitude of the tensor power spectrum, and the residual E -to- B lensing power after delensing, respectively. In the simplest case, foreground parameters include the amplitude, spectral tilts as a function of angular scale, and spectral indices for each component, as well as a free correlation coefficient between dust and synchrotron. All these parameters, including r and A_{lens} are free to vary in the model. To account for foreground frequency decorrelation, caused for example by spectral index variations, we use the minimal moment expansion method presented in Azzoni et al. (2021), which has been shown to describe a wide range of foreground models with varying levels of complexity (Azzoni et al. 2021, W24, Liu et al. 2025). The general moment expansion approach, as proposed in the literature (Chluba et al. 2017; Mangilli et al. 2021; Vacher et al. 2025) accounts for spatial variability in foreground spectra as a source of decorrelation in a perturbative manner, with the implementation used here corresponding to the minimal expansion in terms of model complexity (Azzoni et al. 2021). The model introduces four additional parameters, an amplitude and spectral tilt for each foreground component, characterising the spatial variability of the spectral indices for both components. When presenting our results below, the constraints obtained assuming the simpler foreground model will be labelled “no FG decorr.”, while those using the moment expansion model to characterise frequency decorrelation will be labelled “with FG decorr.”.

We derive constraints on all model parameters, including A_{lens} and r , by sampling the Gaussian likelihood described above using the affine-invariant Markov-chain Monte-Carlo sampler `emcee` (Foreman-Mackey et al. 2013). We also find the best-fit model parameters by maximising the likelihood using Powell’s method (Powell 1964) as implemented in `scipy` (Virtanen et al. 2020). We do this for a subset of 10 simulations, extracting the standard deviation on r from the resulting chains, and calculating the average σ_r across all simulations. We verify that, in all cases explored here, the best-fit value of r recovered is compatible with the input value $r = 0$.

3.2 Results

Fig. 2 shows the forecasted sensitivity of SO to the CMB B -mode power spectrum. The figure shows the B -mode bandpowers averaged over all 500 realisations used for covariance matrix estimation, together with its statistical uncertainties. Note that we do not show the measurements at a particular frequency, but rather the CMB-only bandpowers, reconstructed

⁴ “Pairs of distinct angular bandpowers” refers to cases where the two bandpowers within a pair correspond to different multipole ranges.

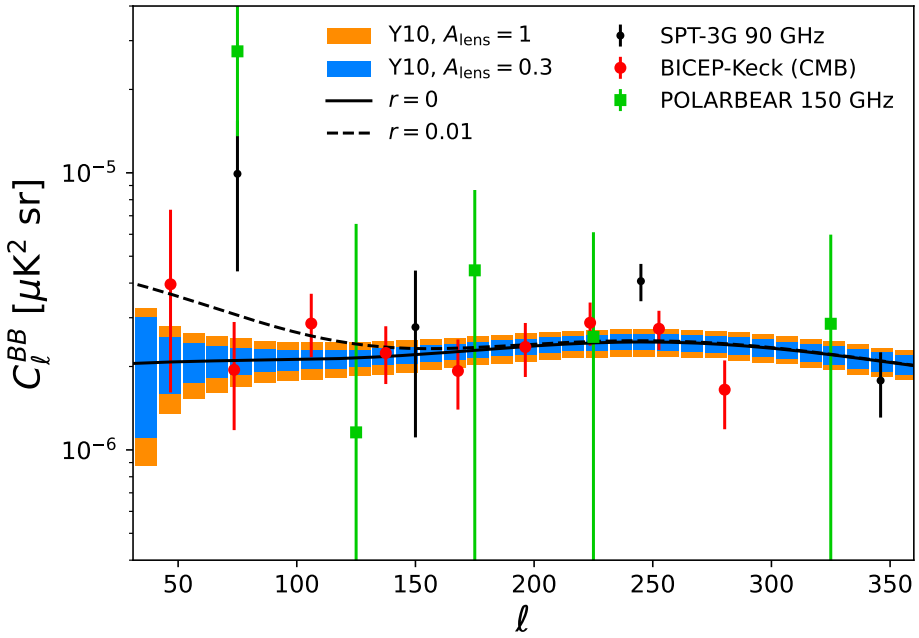


Figure 2. The B -mode power spectrum and uncertainties achievable by SO, accounting for the expansions described in Section 2. Bandpowers of width $\Delta\ell = 10$ are shown after 10 years of observations assuming no delensing (orange bands) and 70% delensing (blue bands), and assuming the “pessimistic” $1/f$ noise model (see Section 3.1 for details). The solid line shows the lensing B -mode power spectrum in the absence of tensor modes ($r = 0$). The signal for $r = 0.01$ is shown in dashed black. Current measurements from BICEP/Keck (red, showing CMB bandpowers, Ade et al. 2021), SPT-3G (black, showing bandpowers at 90 GHz, Zebrowski et al. 2025), and POLARBEAR (green, showing bandpowers at 150 GHz, Adachi et al. 2022) are also shown for reference.

from the multi-frequency spectra assuming knowledge of the foreground spectral indices. The bandpower measurements are shown for the “pessimistic” $1/f$ noise model after 10 years of observations, assuming no delensing ($A_{\text{lens}} = 1$, orange bands) and 70% delensing ($A_{\text{lens}} = 0.3$, blue bands). We also show the theoretical prediction for the lensing B -mode spectrum in the absence of tensor modes ($r = 0$), as well as the signal for $r = 0.01$. In this case, the primordial B -mode signal would be detected at high significance. For reference, the figure also shows current measurements of the B -mode power spectrum at 90 GHz from the South Pole Telescope (SPT-3G, Zebrowski et al. 2025), at 150 GHz from POLARBEAR (Adachi et al. 2022), and the component-separated CMB bandpowers from the BICEP/Keck collaboration (Ade et al. 2021).

Figure 3 shows the forecast uncertainty on r as a function of the total observing time, starting after the third year of observations. The numerical values of σ_r presented in the plot after 5 and 10 years of observations are provided in Table 2. Results are shown assuming both 70% and 50% delensing, in each case presenting constraints for different combinations of assumptions regarding $1/f$ noise and the level of foreground frequency decorrelation. Frequency decorrelation plays an important role in the final constraints, which are degraded by approximately 20% with respect to the case with no frequency decorrelation in the model. However, correlated noise has a stronger impact, with a 30% increase in σ_r when adopting the “pessimistic” $1/f$ noise model. Although the impact of delensing is relatively small at

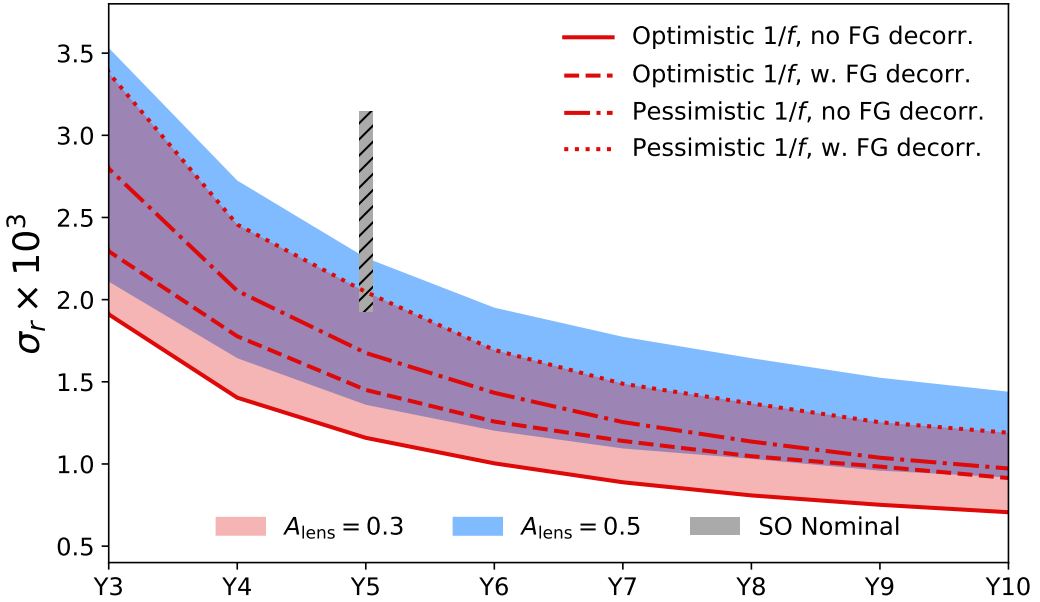


Figure 3. The forecasted 68% constraints on the tensor-to-scalar ratio r , achievable by SO, as a function of time, accounting for the expansions described in Section 2. “YN” denotes the N -th year after the start of observations. Results are shown assuming 50% and 70% delensing (blue and red, respectively), for different assumptions regarding $1/f$ noise and foreground decorrelation. Each band covers the range of σ_r between the worst- and best-case scenarios (the “pessimistic” $1/f$ noise model with foreground frequency decorrelation as described by the moment expansions vs. the “optimistic” $1/f$ noise model and no decorrelation). The constraints that the nominal SO configuration would have been able to attain, with the same foreground and noise assumptions, and $A_{\text{lens}} = 0.5$, are shown as the gray hashed band.

$1/f$ noise	A_{lens}	Survey configuration	$10^3 \times \sigma_r$ no FG decorr.	$10^3 \times \sigma_r$ with FG decorr.
Pessimistic	0.5	Nominal SO	2.7	3.1
		5 years	1.9	2.3
		10 years	1.2	1.4
	0.3	5 years	1.7	2.0
		10 years	1.0	1.2
Optimistic	0.5	Nominal SO	1.9	2.5
		5 years	1.4	1.7
		10 years	0.9	1.1
	0.3	5 years	1.2	1.5
		10 years	0.7	0.9

Table 2. Forecasted 68% constraints on the tensor-to-scalar ratio r achievable by SO, accounting for the expansions described in Section 2, after 5 and 10 years of observations. Results are shown for different assumptions regarding $1/f$ noise and the impact of foreground frequency decorrelation (as characterised by a moments expansion). For comparison, also presented are the constraints forecasted for the nominal SO configuration, without the new SATs studied here, after 5 years of observations, and assuming 50% delensing.

first (of order a few % improvement in σ_r after one year in the most optimistic scenario), achieving the more ambitious 70% delensing efficiency becomes more important towards the end of the survey, when the reduced noise levels make the impact of lensing on the final uncertainties more relevant. In this case, after a 10-year survey, going from $A_{\text{lens}} = 0.5$ to $A_{\text{lens}} = 0.3$ leads to a 20% improvement on the final constraints. The results obtained by the nominal SO setup after 5 years, assuming 50% delensing, are shown as the vertical gray hatched band, which spans the same range of scenarios as the coloured bands.

As summarised in Table 2 we find that, in the most conservative scenario that we have considered (the “pessimistic” $1/f$ noise model, 50% delensing, and accounting for foreground decorrelation), SO will be able to constrain the tensor-to-scalar ratio at the level of $\sigma_r = 0.0014$ after 10 years of observations. We consider this most conservative scenario as our fiducial case. Forecasted constraints improve by 50% to $\sigma_r = 0.0007$ for the “optimistic” $1/f$ noise model, with 70% delensing, and assuming no decorrelation. Our fiducial constraints correspond to a 40% improvement with respect to the bounds that would be achieved after 5 years of observations in the same scenario. These 5-year constraints are themselves 40% tighter than those that would be achieved by the nominal SO configuration after the same observing time. Thus, in combination with the extended 10-year campaign, the upgraded SO SAT complement will improve the nominal SO constraints on primordial B -modes by a factor 2.6, assuming 70% delensing.

Finally, it is interesting to compare the impact these improved constraints on primordial tensor fluctuations will have on models of inflation. Fig. 4 shows the 95% constraints achievable by SO in the n_s – r plane, where n_s is the scalar spectral index. The forecasted n_s uncertainty, $\sigma(n_s) = 0.002$, corresponds to the constraint achievable by the SO LAT (see [SO Collaboration 2025](#) for details), assuming a standard recombination history ([Ali-Haïmoud & Hirata 2011](#); [Chluba & Thomas 2011](#)). Results are shown for the full 10-year SO SAT survey (accounting for the expansions described in Section 2), for two cases: (i) assuming the “pessimistic” $1/f$ noise model and allowing for foreground frequency decorrelation, and (ii) assuming the “optimistic” $1/f$ noise model and no foreground frequency decorrelation. In both cases $A_{\text{lens}} = 0.3$ is assumed. For comparison, results are also shown for the nominal (5-year) SO SAT survey, for the “optimistic” $1/f$ noise model, without allowing for foreground frequency decorrelation, and assuming $A_{\text{lens}} = 0.5$. For illustrative purposes, we assume an inflationary signal corresponding to that predicted by Starobinsky inflation ([Starobinskii 1979](#)) for a total of $N_* = 57$ e -folds of inflation (which recovers the value of $n_s = 0.965$ preferred by *Planck* ([Planck Collaboration 2020a](#))). We see that, while the nominal SO survey would not be able to detect this signal (corresponding to $r = 0.0037$), the full 10-year SO SAT survey could provide evidence at the 3σ confidence level or higher. The figure also shows the current constraints from BICEP/Keck ([Ade et al. 2021](#)).

4 Summary

This paper presents updated forecasts for constraints on the tensor-to-scalar ratio r from the Simons Observatory. Compared to the original SO SAT configuration used for our previous forecasts ([SO Collaboration 2019](#)), the updated forecasts incorporate the addition of two further SATs operating in the MF bands (93/145 GHz), and the addition of one further telescope platform, which will allow continuous operation of the SO LF band (27/39 GHz) receiver until the end of the survey. In addition, an extension of the SO SAT survey duration to 2035 is considered. The two new MF SATs will exploit new detector technology, using

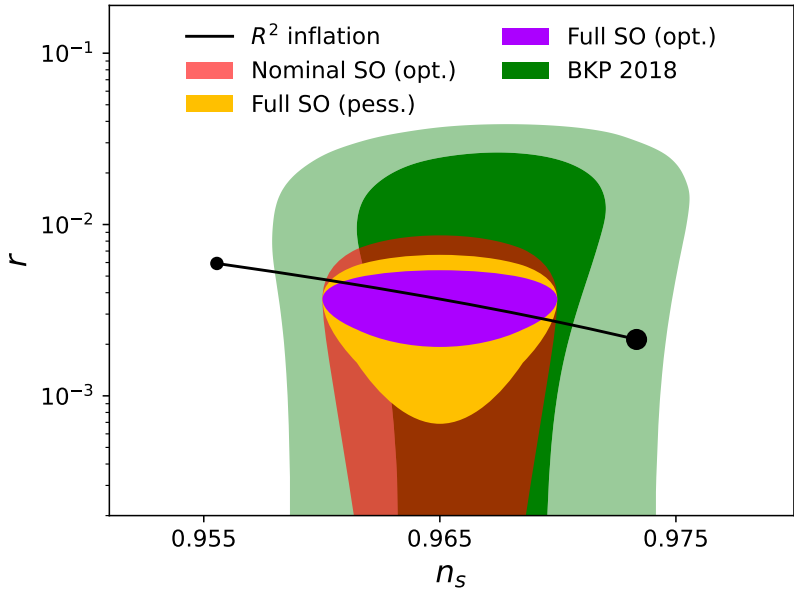


Figure 4. The forecasted 95% constraints on the tensor-to-scalar ratio r and the scalar spectral index n_s that could be achieved by SO. Results are shown for the full SO SAT configuration, including the enhancements detailed in Section 2, assuming 10 years of observation and 70% delensing. These forecasts are presented for two cases: (i) assuming the “pessimistic” $1/f$ noise model and allowing for foreground frequency decorrelation (yellow), and (ii) assuming the “optimistic” $1/f$ noise model and no frequency decorrelation (purple). The black line shows the prediction from R^2 inflation (Starobinsky model) for a total number of e -folds in the range $45 < N_* < 75$, with the range limits marked by the small and large black circles. We have assumed the true value of r to correspond to the Starobinsky prediction given the best-fit value of n_s preferred by *Planck* (Planck Collaboration 2020a). For comparison, the red contours show the 95% constraints achievable by the nominal SO SAT configuration (assuming a 5-year survey and 50% delensing, as well as optimistic $1/f$ noise and no frequency decorrelation), while the green contours show the current 68% and 95% constraints from BICEP/Keck, *Planck*, and WMAP data (Ade et al. 2021).

KIDs in place of TESs, and will double the mapping speed of the SO SAT survey at 93 and 145 GHz. Continuous operation of the LF SAT will complement the frequency coverage of the experiment, providing key additional sensitivity to synchrotron contamination. These enhancements will result in a 40% increase in the sensitivity to primordial tensor modes with respect to the nominal SO configuration after 5 years of observation, and a 70% increase after a 10-year campaign. The final constraints on r will depend critically on the level of foreground contamination, large-scale instrumental and atmospheric noise, and other instrumental systematic effects. In particular, frequency decorrelation of the Galactic foreground components can degrade final constraints by up to 30% in the most optimistic scenario (i.e. assuming the “optimistic” $1/f$ noise model and 70% delensing). Given the sensitivity and sky coverage that SO will achieve, accounting for frequency decorrelation will likely be unavoidable. Likewise, large-scale $1/f$ noise has a significant impact on the final B -mode constraints, degrading the bounds on r by 25–30% when comparing the “optimistic” and “pessimistic” noise models of SO Collaboration (2019). Finally, as the instrumental sensitivity grows, delensing will become increasingly necessary. After 10 years of observations, the SO constraints on r may improve by around 20% if the delensing efficiency is increased from 50% to 70%.

The SO SAT survey is already underway using the first two MF SATs. More recently, commissioning of the third SAT, operating at UHF (225/280 GHz), has begun. Preliminary analysis of the first data from these SATs is ongoing and initial findings on the instrument characterisation and performance will be reported in the near future. However, it is currently too early in the analysis phase to comment on the degree to which the large-scale noise properties of the observations, the complexity of Galactic foregrounds, and the levels of delensing achieved, will ultimately compare to the assumptions used for the forecasts presented here. The two additional MF SATs and the LF SAT are expected to begin operations in 2027. By this time, several SAT-years worth of survey data will have been collected with the first three SATs. In addition to delivering SO’s first constraints on r , these early survey data will be extremely valuable for understanding the properties of the observations, and of the foregrounds in the targeted sky area. These can then be used to inform survey strategy choices for subsequent operations with the full six-telescope SO SAT configuration.

Acknowledgments

This work was supported by the United Kingdom Research and Innovation (UKRI) Infrastructure Fund and by the Science and Technology Facilities Council (STFC) (grant numbers ST/X006336/1, SMHT/X006352/1, ST/X006379/1, ST/X006344/1, ST/X006360/1, ST/X006387/1, ST/X006395/1, ST/X006328/1). This work was supported in part by a grant from the Simons Foundation (Award #457687, B.K.). This work was supported by the U.S. National Science Foundation (Award Number: 2153201). This work was also supported by JSPS KAKENHI Grant Numbers JP22H04913, JP23H00105, JP24K23938, JP25H00403. AC acknowledges support from the STFC (grant numbers ST/W000997/1 and ST/X006387/1). GG acknowledges the support by the MUR PRIN2022 Project “BROWSEPOL: Beyond standaRd mOdel With coSmic microwavE background POLarization”-2022EJNZ53 financed by the European Union - Next Generation EU. MG, ML, PN, LP, GZ and GG acknowledge the financial support from the INFN InDark initiative and from the COSMOS network through the ASI (Italian Space Agency) Grants 2016-24-H.0 and 2016-24-H.1-2018. MG, ML, MM are funded by the European Union (ERC, RELiCS, project number 101116027). MG and MF acknowledges support from the PRIN (Progetti di ricerca di Rilevante Interesse Nazionale) number 2022WJ9J33. RB, JEG, AAK, and XR acknowledge funding from the European Union (ERC, CMBeam, 101040169) and support from the University of Iceland Research Fund. MH acknowledges support from the National Science and Technology Council and the Ministry of Education of Taiwan. The research was carried out in part at the Jet Propulsion Laboratory, California Institute of Technology, under a contract with the National Aeronautics and Space Administration (80NM0018D0004). ADH acknowledges support from the Sutton Family Chair in Science, Christianity and Cultures, from the Faculty of Arts and Science, University of Toronto, and from the Natural Sciences and Engineering Research Council of Canada (NSERC; RGPIN-2023-05014, DGECR-2023-00180). RH acknowledges support from the NSERC Canada Discovery Grant Program RGPIN-2025-06483 and the Connaught Fund. The Dunlap Institute is funded through an endowment established by the David Dunlap family and the University of Toronto. This document was prepared by Simons Observatory using the resources of the Fermi National Accelerator Laboratory (Fermilab), a U.S. Department of Energy, Office of Science, Office of High Energy Physics HEP User Facility. Fermilab is managed by Fermi Forward Discovery Group, LLC, acting under Contract No. 89243024CSC000002. CS acknowledges support from the Agencia Nacional de Inves-

tigación y Desarrollo (ANID) through Basal project FB210003. FN acknowledges funding from the European Union (ERC, POLOCALC, 101096035). CLR acknowledges support from the Australian Research Council's Discovery Project scheme (No. DP210102386). AB, BB, SB, PC, JE, WK, WS, ETKS, and AVA were supported by the SCIPOL project,⁵ funded by the European Research Council (ERC) under the European Union's Horizon 2020 research and innovation programme (PI: J. Errard, Grant No. 101044073).

References

Adachi, S., et al. 2022, [arXiv:2203.02495](https://arxiv.org/abs/2203.02495), *Ap. J.*, **931**, 101, Improved Upper Limit on Degree-scale CMB B-mode Polarization Power from the 670 Square-degree POLARBEAR Survey

Addamo, G., et al. 2021, [arXiv:2008.11049](https://arxiv.org/abs/2008.11049), *JCAP*, **2021**, 008, The large scale polarization explorer (LSPE) for CMB measurements: performance forecast

Ade, P. A. R., et al. 2021, [arXiv:2110.00483](https://arxiv.org/abs/2110.00483), *Phys. Rev. Lett.*, **127**, 151301, Improved Constraints on Primordial Gravitational Waves using Planck, WMAP, and BICEP/Keck Observations through the 2018 Observing Season

—. 2022, [arXiv:2103.13334](https://arxiv.org/abs/2103.13334), *Ap. J.*, **927**, 174, A Constraint on Primordial B-modes from the First Flight of the SPIDER Balloon-borne Telescope

Ali-Haïmoud, Y. & Hirata, C. M. 2011, [arXiv:1011.3758](https://arxiv.org/abs/1011.3758), *Phys. Rev. D*, **83**, 043513, HyRec: A fast and highly accurate primordial hydrogen and helium recombination code

Alonso, D., Sanchez, J., Slosar, A., & LSST Dark Energy Science Collaboration. 2019, [arXiv:1809.09603](https://arxiv.org/abs/1809.09603), *MNRAS*, **484**, 4127, A unified pseudo- C_ℓ framework

Azzoni, S., Abitbol, M. H., Alonso, D., Gough, A., Katayama, N., & Matsumura, T. 2021, [arXiv:2011.11575](https://arxiv.org/abs/2011.11575), *JCAP*, **2021**, 047, A minimal power-spectrum-based moment expansion for CMB B-mode searches

Battistelli, E. S., et al. 2020, [arXiv:2001.10272](https://arxiv.org/abs/2001.10272), *Journal of Low Temperature Physics*, **199**, 482, QUBIC: The Q & U Bolometric Interferometer for Cosmology

Bhandarkar, T., et al. 2025, [arXiv:2501.09241](https://arxiv.org/abs/2501.09241), *Ap. J. Supp.*, **279**, 34, Simons Observatory: Characterization of the Large Aperture Telescope Receiver

BICEP2/Keck Collaborations. 2018, [arXiv:1810.05216](https://arxiv.org/abs/1810.05216), *Phys. Rev. Lett.*, **121**, 221301, Constraints on Primordial Gravitational Waves Using Planck, WMAP, and New BICEP2/Keck Observations through the 2015 Season

Chluba, J., Hill, J. C., & Abitbol, M. H. 2017, [arXiv:1701.00274](https://arxiv.org/abs/1701.00274), *MNRAS*, **472**, 1195, Rethinking CMB foregrounds: systematic extension of foreground parametrizations

Chluba, J. & Thomas, R. M. 2011, [arXiv:1010.3631](https://arxiv.org/abs/1010.3631), *MNRAS*, **412**, 748, Towards a complete treatment of the cosmological recombination problem

Day, P. K., LeDuc, H. G., Mazin, B. A., Vayonakis, A., & Zmuidzinas, J. 2003, *Nature*, **425**, 817, A broadband superconducting detector suitable for use in large arrays

Doyle, S., Mauskopf, P., Naylor, J., Porch, A., & Duncombe, C. 2008, *Journal of Low Temperature Physics*, **151**, 530, Lumped Element Kinetic Inductance Detectors

Foreman-Mackey, D., Hogg, D. W., Lang, D., & Goodman, J. 2013, [arXiv:1202.3665](https://arxiv.org/abs/1202.3665), *Publications of the Astronomical Society of the Pacific*, **125**, 306, emcee: The MCMC Hammer

Galitzki, N., et al. 2024, [arXiv:2405.05550](https://arxiv.org/abs/2405.05550), *Ap. J. Supp.*, **274**, 33, The Simons Observatory: Design, Integration, and Testing of the Small Aperture Telescopes

⁵<https://scipol.in2p3.fr>

Ghosh, S., et al. 2022, [arXiv:2205.14804](https://arxiv.org/abs/2205.14804), *JCAP*, **2022**, 063, Performance forecasts for the primordial gravitational wave detection pipelines for AliCPT-1

Harrington, K., et al. 2016, [arXiv:1608.08234](https://arxiv.org/abs/1608.08234), in Society of Photo-Optical Instrumentation Engineers (SPIE) Conference Series, Vol. 9914, Millimeter, Submillimeter, and Far-Infrared Detectors and Instrumentation for Astronomy VIII, ed. W. S. Holland & J. Zmuidzinas, 99141K

Hensley, B. S., et al. 2022, [arXiv:2111.02425](https://arxiv.org/abs/2111.02425), *Ap. J.*, **929**, 166, The Simons Observatory: Galactic Science Goals and Forecasts

Hertig, E., et al. 2024, [arXiv:2405.01621](https://arxiv.org/abs/2405.01621), *Phys. Rev. D*, **110**, 043532, The Simons Observatory: Combining cross-spectral foreground cleaning with multitracer B-mode delensing for improved constraints on inflation

Hervías-Caimapo, C., et al. 2025, [arXiv:2502.00946](https://arxiv.org/abs/2502.00946), *JCAP*, **2025**, 055, The Simons Observatory: validation of reconstructed power spectra from simulated filtered maps for the small aperture telescope survey

Hui, H., et al. 2018, [arXiv:1808.00568](https://arxiv.org/abs/1808.00568), in Society of Photo-Optical Instrumentation Engineers (SPIE) Conference Series, Vol. 10708, Millimeter, Submillimeter, and Far-Infrared Detectors and Instrumentation for Astronomy IX, ed. J. Zmuidzinas & J.-R. Gao, 1070807

Jung, G., Racine, B., & van Tent, B. 2018, [arXiv:1810.01727](https://arxiv.org/abs/1810.01727), *JCAP*, **2018**, 047, The bispectra of galactic CMB foregrounds and their impact on primordial non-Gaussianity estimation

Kamionkowski, M., Kosowsky, A., & Stebbins, A. 1997, *Phys. Rev. Lett.*, **78**, 2058, A Probe of Primordial Gravity Waves and Vorticity, <https://link.aps.org/doi/10.1103/PhysRevLett.78.2058>

Lee, A. T., et al. 2008, in American Institute of Physics Conference Series, Vol. 1040, KEK CosmoPhysics Group Inaugural Conference “Accelerators in the Universe”: Interplay between High Energy Physics and CosmoPhysics, ed. H. Kodama & K. Ioka (AIP), 66–77

LiteBIRD Collaboration. 2023, [arXiv:2202.02773](https://arxiv.org/abs/2202.02773), *Progress of Theoretical and Experimental Physics*, **2023**, 042F01, Probing cosmic inflation with the LiteBIRD cosmic microwave background polarization survey

Liu, C., Jones, M. E., & Taylor, A. C. 2021, [arXiv:2011.05691](https://arxiv.org/abs/2011.05691), *MNRAS*, **501**, 5096, Characterizing the performance of high-speed data converters for RFSoC-based radio astronomy receivers

Liu, Y., et al. 2025, [arXiv:2508.00073](https://arxiv.org/abs/2508.00073), *JCAP*, **2025**, 024, The Simons Observatory: assessing the impact of dust complexity on the recovery of primordial B-modes

Mangilli, A., Aumont, J., Rotti, A., Boulanger, F., Chluba, J., Ghosh, T., & Montier, L. 2021, [arXiv:1912.09567](https://arxiv.org/abs/1912.09567), *Ast. and Ap.*, **647**, A52, Dust moments: towards a new modeling of the galactic dust emission for CMB B-modes analysis

Martínez-Solaeche, G., Karakci, A., & Delabrouille, J. 2018, [arXiv:1706.04162](https://arxiv.org/abs/1706.04162), *MNRAS*, **476**, 1310, A 3D model of polarized dust emission in the Milky Way

Namikawa, T., et al. 2022, [arXiv:2110.09730](https://arxiv.org/abs/2110.09730), *Phys. Rev. D*, **105**, 023511, Simons Observatory: Constraining inflationary gravitational waves with multitracer B-mode delensing

Planck Collaboration. 2020a, [arXiv:1807.06209](https://arxiv.org/abs/1807.06209), *Ast. and Ap.*, **641**, A6, Planck 2018 results. VI. Cosmological parameters

—. 2020b, [arXiv:1807.06210](https://arxiv.org/abs/1807.06210), *Ast. and Ap.*, **641**, A8, Planck 2018 results. VIII. Gravitational lensing

Powell, M. J. D. 1964, <https://academic.oup.com/comjnl/article-pdf/7/2/155/959784/070155.pdf>, *The Computer Journal*, **7**, 155, An efficient method for finding the minimum of a function of several variables without calculating derivatives, <https://doi.org/10.1093/comjnl/7.2.155>

Seljak, U. & Zaldarriaga, M. 1997, [astro-ph/9609169](https://arxiv.org/abs/astro-ph/9609169), *Phys. Rev. Lett.*, **78**, 2054, Signature of Gravity Waves in the Polarization of the Microwave Background

Smith, K. M. 2006, [astro-ph/0511629](#), *Phys. Rev. D*, **74**, 083002, Pseudo- C_ℓ estimators which do not mix E and B modes

SO Collaboration. 2019, [arXiv:1808.07445](#), *JCAP*, **2019**, **056**, The Simons Observatory: science goals and forecasts

—. 2025, [arXiv:2503.00636](#), *JCAP*, **2025**, **034**, The Simons Observatory: science goals and forecasts for the enhanced Large Aperture Telescope

Starobinskii, A. A. 1979, Soviet Journal of Experimental and Theoretical Physics Letters, **30**, 682, Spectrum of relict gravitational radiation and the early state of the universe

Stebor, N., et al. 2016, in Society of Photo-Optical Instrumentation Engineers (SPIE) Conference Series, Vol. 9914, Millimeter, Submillimeter, and Far-Infrared Detectors and Instrumentation for Astronomy VIII, ed. W. S. Holland & J. Zmuidzinas, 99141H

Swetz, D. S., et al. 2011, [arXiv:1007.0290](#), *Ap. J. Supp.*, **194**, 41, Overview of the Atacama Cosmology Telescope: Receiver, Instrumentation, and Telescope Systems

The Pan-Experiment Galactic Science Group. 2025, [arXiv:2502.20452](#), *Ap. J.*, **991**, 23, Full-sky Models of Galactic Microwave Emission and Polarization at Subarcminute Scales for the Python Sky Model

Thorne, B., Dunkley, J., Alonso, D., & Næss, S. 2017, [arXiv:1608.02841](#), *MNRAS*, **469**, 2821, The Python Sky Model: software for simulating the Galactic microwave sky

Vacher, L., Carones, A., Aumont, J., Chluba, J., Krachmalnicoff, N., Ranucci, C., Remazeilles, M., & Rizzieri, A. 2025, [arXiv:2411.11649](#), *Ast. and Ap.*, **697**, A212, How bad could it be? Modelling the 3D complexity of the polarised dust signal using moment expansion

Virtanen, P., et al. 2020, [arXiv:1907.10121](#), *Nature Methods*, **17**, 261, SciPy 1.0: fundamental algorithms for scientific computing in Python

von Hausegger, S., Gammelgaard Ravnebjerg, A., & Liu, H. 2019, [arXiv:1811.02470](#), *MNRAS*, **487**, 5814, Statistical properties of polarized CMB foreground maps

Wang, J., Jaffe, T. R., Enßlin, T. A., Ullio, P., Ghosh, S., & Santos, L. 2020, [arXiv:1907.00207](#), *Ap. J. Supp.*, **247**, 18, hammurabi X: Simulating Galactic Synchrotron Emission with Random Magnetic Fields

Wolz, K., et al. 2024, [arXiv:2302.04276](#), *Ast. and Ap.*, **686**, A16, The Simons Observatory: Pipeline comparison and validation for large-scale B-modes

Xu, Z., et al. 2021, [arXiv:2104.09511](#), *Research Notes of the American Astronomical Society*, **5**, 100, The Simons Observatory: The Large Aperture Telescope (LAT)

Yu, B., Hill, J. C., & Sherwin, B. D. 2017, [arXiv:1705.02332](#), *Phys. Rev. D*, **96**, 123511, Multitracer CMB delensing maps from Planck and WISE data

Yu, C., et al. 2023, [arXiv:2208.10523](#), *Review of Scientific Instruments*, **94**, 014712, SLAC microresonator RF (SMuRF) electronics: A tone-tracking readout system for superconducting microwave resonator arrays

Zebrowski, J. A., et al. 2025, [arXiv:2505.02827](#), *arXiv e-prints*, [arXiv:2505.02827](#), Constraints on Inflationary Gravitational Waves with Two Years of SPT-3G Data

Zhu, N., et al. 2021, [arXiv:2103.02747](#), *Ap. J. Supp.*, **256**, 23, The Simons Observatory Large Aperture Telescope Receiver